Effect of simulated brazing on the microstructure and corrosion behavior of twin roll cast AA3003

Verkens, Donovan ; Revilla, Reynier I.; Kosari, Ali; Günyüz, Mert ; Işıksaçan, Cemil ; Mol, Arjan; De Graeve, Iris; Terryn, Herman

DOI
10.1002/maco.201911053

Publication date
2020

Document Version
Final published version

Published in
Materials and Corrosion

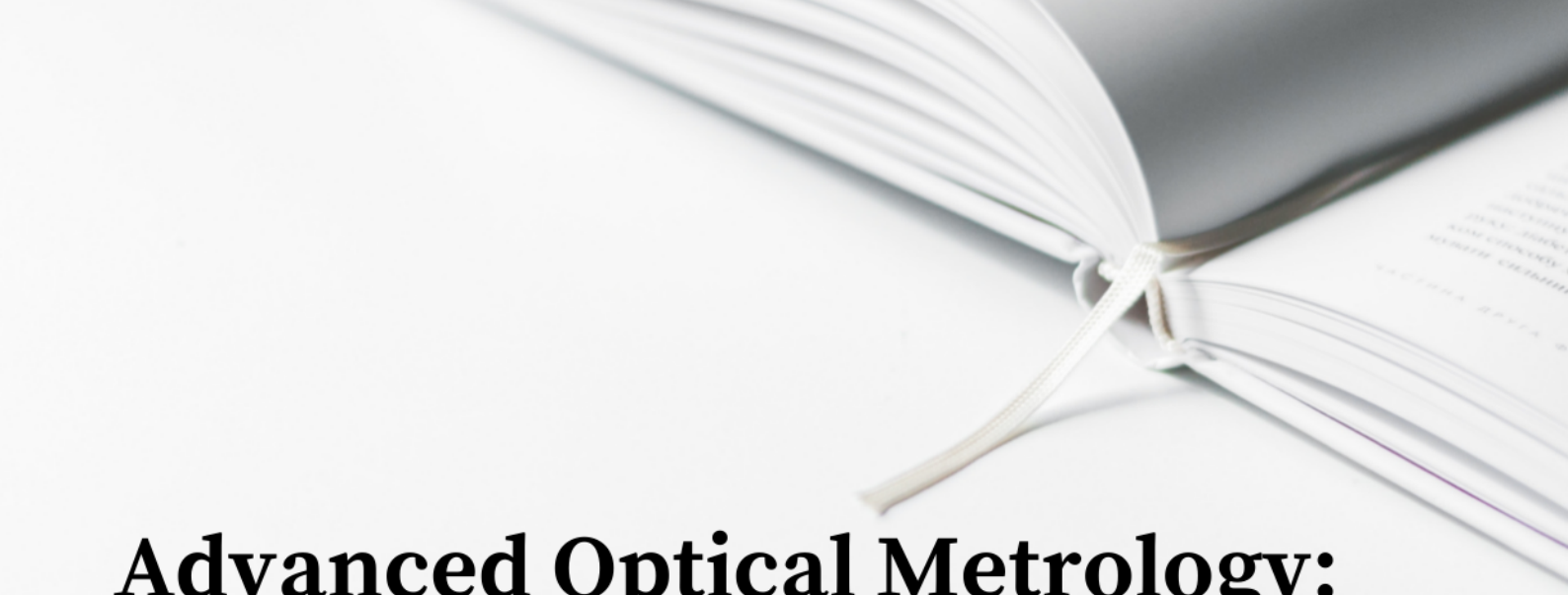

Advanced Optical Metrology: Corrosion now available

Free educational eBook

Corrosion is a natural process consisting of the chemical, biochemical, or electrochemical reaction between a given material and its environment, producing a deterioration of the material and its functional properties. Because of this, corrosion is one of the most common ways that a material fails.

Today, the demands on materials' corrosion resistance are increasing to improve operational reliability and extend product life.

Download our free eBook to learn more.

Download it now

This eBook is sponsored by OLYMPUS

WILEY

Received: 5 June 2019 | Accepted: 20 June 2019

DOI: 10.1002/maco.201911053

ARTICLE

Materials and Corrosion

Effect of simulated brazing on the microstructure and corrosion behavior of twin roll cast AA3003

Donovan Verkens[1] | Reynier I. Revilla[1] | Ali Kosari[2] | Mert Günyüz[3] | Cemil Işıksaçan[3] | Johannes M.C. Mol[2] | Iris De Graeve[1] | Herman Terryn[1]

[1]Electrochemical and Surface Engineering (SURF), Vrije Universiteit Brussel (VUB), Brussels, Belgium

[2]Department of Materials Science and Engineering, Delft University of Technology, Delft, The Netherlands

[3]R&D, Assan Alüminyum A.Ş., Istanbul, Turkey

Correspondence
Donovan Verkens, Electrochemical and Surface Engineering (SURF), Vrije Universiteit Brussel (VUB), 1050 Brussels, Belgium.
Email: Donovan.verkens@vub.be

Abstract

Aluminum alloy (AA) 3003 is widely used as fin and tube material in heat exchangers. In these heat exchangers, the tube and fin material are brazed together by means of an AA4xxx alloy. In this study, the effect of a simulated brazing step on the microstructure and corrosion behavior of a twin roll casted (TRC) AA3003 was studied. In particular, the effect of simulated brazing on the corrosion properties of the centre line segregation (CLS) of alloying elements and the interaction of the intermetallic particles with the surrounding matrix is explored. It is shown that the cross sections are significantly more active than the surface of the TRC AA3003, revealing the importance of the CLS on the corrosion behavior. Furthermore, it is shown that the number of pits and their depths decreased considerably on the exposed cross sections after simulated brazing, especially near the CLS. Scanning Kelvin probe force microscopy measurements show that after the simulated brazing step the Volta potential difference between the intermetallic particles and the matrix reduced significantly. This change in the Volta potential could be caused by the slight increase of Si content in the matrix.

KEYWORDS

AA3003, brazing, corrosion, twin roll casting

1 | INTRODUCTION

A continuous casting technique like twin roll casting (TRC) is a very novel and competitive technique to produce flat-rolled aluminum products. Unlike for direct chill (DC) casting, TRC produces less waste and does not need the high investment cost of hot rolling facilities. In TRC the molten aluminum alloy (AA) is fed by a ceramic nozzle to two counter-rotating and water-cooled steel rolls. A schematic representation of the TRC process is shown in Figure 1. In the rolling gap of these twin rolls, the molten AA solidifies and undergoes, to some extent, a hot rolling process step to form a strip. However, despite the higher cooling rates than in DC-casting, TRC is known to result in macrosegregation of alloying elements towards the centre plane of the casted strip. This macrosegregation, referred to as centre line segregation (CLS), cannot be removed from the casted strip.[1,2] DC-casted material also shows a macrosegregation, but towards the outer layers of the ingot.[3] Unlike the CLS in TRC, the macrosegregation in DC-casting can and is removed by scalping before hot rolling of the ingots to a strip. Besides the difference in macrosegregation, TRC material is known to have significantly smaller grain sizes after casting, higher solid-solution supersaturation and a finer dispersion of primary particles compared to

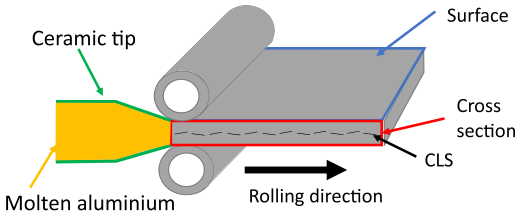

FIGURE 1 Schematic of the TRC process and the two surfaces analyzed: along the surface of the flat-rolled foil and a cross-section along the rolling direction, respectively marked in blue and red. TRC, twin roll casting [Color figure can be viewed at wileyonlinelibrary.com]

DC-casted material.[4] Furthermore, it is well known that hot rolling after DC-casting leads to the formation of a near-surface deformed layer, which is not the case in TRC.[5]

The AA3003, either produced by TRC or DC-casting and subsequent hot-rolling, is used widely as fin material in heat exchangers. In these heat exchangers, the tube and fin material are brazed together by means of an AA4xxx alloy, that has a eutectic temperature lower than the melting temperature of the fin and tube material.[6]

The corrosion properties of the DC-casted and subsequent hot-rolled AA3003 have already been studied substantially in the past.[7–10] A statistical evaluation of the susceptibility to pitting corrosion of DC-casted and subsequent hot-rolled AA3003 reported a high pitting factor, indicating a highly localized corrosion process in a saline environment.[7] Davoodi et al.[9] investigated, the localized activity at the surface of DC-casted and subsequent hot-rolled AA3003 in a saline solution by means of integrated atomic force microscopy and scanning electrochemical microscopy (AFM/SECM). The combined AFM and SECM technique showed the cathodic activity of the intermetallic particles and the increased anodic current during anodic polarization due to the localized dissolution adjacent to some of the larger intermetallic particles. The in-situ AFM measurements in an acetic acid solution at OCP also reported the localized dissolution of the aluminum matrix adjacent to the intermetallic particles and the formation of deposits of ring-like corrosion products. Furthermore, it was reported that for the alloy studied, the larger intermetallic particles cause more localized corrosion than the submicrometric dispersoids.[9] By using scanning Kelvin probe force microscopy (SKPFM), Davoodi et al.[8] also showed the cathodic behavior of the intermetallic particles relative to the aluminum matrix in the DC-casted and subsequent hot-rolled AA3003 after brazing. The same authors also reported that the size of the intermetallic particles will determine the Volta potential difference between them and the surrounding aluminum matrix. These SKPFM measurements showed that the larger the intermetallic particle the larger the Volta potential difference will be between them and the matrix. Davoodi et al. attributed the size dependence of the Volta potential of the intermetallic particles to a variation in Fe and Si content in these particles. In situ AFM measurements showed that the fine dispersoids, which were abundant in the brazed alloy, did not induce localized corrosion.[10] The effect of a brazing step on the microstructural and electrochemical properties of a modified DC-casted AA4xxx/AA3xxx brazing sheet was investigated by Afshar et al.[6,11] They reported that the microstructural changes in the modified DC-casted AA4xxx/AA3xxx brazing sheet, due to a brazing step, had the following impact on the corrosion properties: they increased the Volta potential difference of the re-solidified clad matrix, they introduced localized corrosion susceptibility on the brazed clad and core structures and they reduced the cathodic protection power of the re-solidified clad material.[6,11]

On the other hand, little work has been done on TRC AA3003. Işıksaçan et al.[12] studied the effect of the CLS on the corrosion behavior of two types of alloys, namely an AA3003 and an AA8006 alloy, both used in the construction of heat exchangers. Furthermore, the effect of chemical composition (the Zn content in the AA3003 and the Cu content in the AA8006 alloy) and thermo-mechanical processing (different homogenization heat treatments) on the corrosion behavior of the CLS in an HCl–NaCl solution was investigated. The authors reported that the CLS will act as a preferential site for corrosion attack and that the CLS zone in the material has the lowest OCP value compared to other zones in the material. It was also reported that the high Zn-containing AA3003, and the Cu-containing AA8006 alloy with a high homogenization temperature had an increased corrosion activity at the CLS.[12]

However, to the best of our knowledge, the effect of a simulated brazing step on the electrochemical properties of AA3003 fin material produced by TRC has not been investigated yet. Furthermore, the cross-section of this AA3003 fin material is exposed at some locations in heat exchangers, so studying both the outer surface as well as its cross-section is of pivotal importance to gain root cause information on microstructural effects on corrosion performance for the material in its final application. In particular, considering the potential exposure of cross-sectional areas and the relatively high corrosion susceptibility of the CLS, the study of this region is of key importance to understand the microstructural effects on the resulting corrosion mechanisms and kinetics for these materials. Therefore, this study investigates the effect of a simulated brazing step on the microstructure and the corrosion properties of the CLS and the

interaction of the intermetallic particles with the surrounding aluminum matrix. This is carried out through a set of potentiodynamic polarization experiments and immersion tests, which are complemented with a systematic analysis of the pits size and distribution. In addition, SKPFM was used to obtain Volta potential maps of representative areas of the samples surface and linked to the local corrosion behavior of the material.

2 | MATERIALS AND METHODS

2.1 | Samples and simulated brazing procedure

The AA3003 samples, provided by Assan Alüminyum, were produced by twin roll casting. After twin roll casting, the specimens were homogenized, cold rolled, annealed and flat-rolled to a thickness of 70 μm. Part of the samples was subjected to a simulated brazing step. During this brazing step, the samples were heat treated at 600°C for 5 minutes and were then cooled in ambient conditions. Two types of surfaces were analyzed during the experiments: along the surface of the flat-rolled foil and cross sections along the rolling direction, as can be seen in Figure 1. All the samples were mechanically ground and polished, finishing with 0.04 μm standard colloidal silica suspension (OP-S). The chemical composition of the AA3003 was provided by Assan Alüminyum and is shown in Table 1.

2.2 | Electrochemical measurements

All the electrochemical measurements were carried out in a three-electrode cell configuration using an AUTOLAB Potentiostat-Galvanostat (PGSTAT 30). The sample as the working electrode, a platinum counter electrode, and a saturated Ag/AgCl reference electrode. A 0.1 M NaCl solution was used as an electrolyte at room temperature. The open circuit potential (OCP) was monitored for 1 hr at a measuring interval of 0.1 s, so that the system could stabilize before the potentiodynamic polarization measurements. Two types of potentiodynamic polarization tests were performed at a rate of 0.1 V/min: the first starting at 20 mV below OCP towards the positive direction to 1.6 V above OCP and the second starting at 20 mV above OCP in the negative direction to −1.3 V with respect to the reference electrode potential. Different samples were used for these anodic and cathodic polarizations respectively. An automatic current range was selected between 10 nA and 1 A. The potentiodynamic polarization measurements were performed three to five times for each sample. From these measurements, the pitting potential was determined for each sample.

2.3 | Surface characterization

The characterization of the microstructure and the corrosion morphology was done using: optical microscopy (with a Leica DMi8 microscope), scanning electron microscopy/energy dispersive X-ray spectroscopy (SEM/EDS) and high angle annular dark field-scanning TEM (HAADF-STEM)/EDS. For the SEM/EDS analysis, a JOEL JSM-IT300 was used with an acceleration voltage of 20 kV, a working distance of 10 mm and a probe current of 1.2 nA. The statistical analysis of the pits formed during the immersion tests, in 0.1 M NaCl solution for 24 hr, was performed with the Leica Application Suite X (LAS X) software of the optical microscope. This statistical analysis was performed on the SEM images. For the HAADF-STEM/EDS analysis cross-sectional samples were prepared by using an FEI Helios G4 focused ion beam microscope and lift-out procedure. The obtained lamellae were mounted on a copper half-grid and then this grid was loaded on a double-tilt Be TEM holder. An FEI Titan cubed Cs-corrected TEM was operated at 300 kV to perform STEM imaging and EDS mapping. The elemental mappings by HAADF-STEM/EDS, determining the chemical composition of the matrix, were performed before and after the simulated brazing step.

AFM/SKPFM measurements were performed with a Park Systems XE-100 atomic force microscope in ambient conditions. Rectangular conductive cantilevers, ANSCM-PT from AppNano, were used to perform the measurements. These cantilevers have a Pt/Ir coating, a resonant frequency of 50–70 kHz and a spring constant of 1–5 N/m. The scanned area was 40 × 40 μm and the scanning rate was 0.07 Hz. Topography and corresponding potential maps were measured simultaneously by a dynamic mode with a single-pass methodology. The measured potential, contact potential difference (CPD) between the tip of the cantilever and the sample, is associated with the difference between the work

TABLE 1 The chemical composition of the twin roll casted AA3003

Si (wt%)	Fe (wt%)	Mn (wt%)	Mg (wt%)	Zn (wt%)	Cu (wt%)	Zr (wt%)	Al (wt%)
0.70–0.80	0.4–0.50	1.40–1.60	0–0.02	1.40–1.60	0.05–0.10	0.05–0.20	Balance

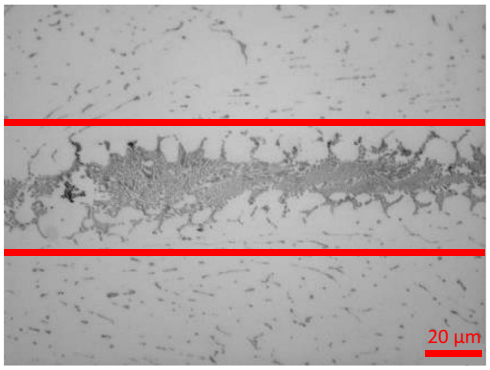

FIGURE 2 Optical image of the cross-section of a casted AA3003 strip, marking the centre line segregation (CLS) with two parallel red lines [Color figure can be viewed at wileyonlinelibrary.com]

function of the tip and the sample. Therefore, this measured signal is directly correlated to the Volta potential of the sample's surface.[13,14] Finally, to report the real relation between the Volta potential values of the sample surface, the measured potential is inverted. All the Volta potential maps were taken on the same day, this was done to assure that the temperature and humidity conditions were the same for all the measurements. The Volta potential mappings were repeated three to four times for each cross-sectional sample.

3 | RESULTS AND DISCUSSION

3.1 | Effect of the CLS on corrosion

As mentioned in Section 1, the twin roll casted (TRC) AA3003 shows a macrosegregation of alloying elements. This macro segregation towards the center plane of the casted strip is known as CLS. This CLS is known to be caused by a liquid flow induced by the production process itself.[1,2] Figure 2 shows an optical image of the cross-section of a casted strip in which the CLS can be clearly observed. The red lines delimiting the CLS in Figure 2 are arbitrarily chosen to highlight this region enriched in intermetallic particles. In Figure 2a TRC strip sample is chosen to show the CLS, which has a thickness of 5.6 mm, and not the 70 µm thick foil sample. This because the CLS is better visible in the strip sample, nevertheless the CLS is very much present in the foil sample.

Potentiodynamic polarization measurements (Figure 3) on the surface of the flat-rolled foil material and the cross-sectional samples were performed in aerated solution. The anodic polarization measurements show for both samples an active behavior with a relatively high increase of current densities upon anodic polarization. Furthermore, these show that a lower limiting current density was obtained for the surface compared to that obtained on the cross-section of the samples. A difference of almost two orders of magnitude was detected, 10^{-3} A cm^{-2} for the surface and 10^{-1} A cm^{-2} for the cross-section. The cathodic polarization measurements (Figure 3) show that the cathodic current densities of the cross-sectional samples are larger compared to the surface samples, at −1.3 V (vs. Ag/AgCl) almost one order of magnitude. The cathodic activity measured in the cathodic polarization plots can be linked with the intermetallic particles that will act cathodically compared to the matrix. In other words, the higher cathodic activity could be caused by the larger number of intermetallic particles per surface area in the cross sections, originating from the CLS. In addition, it is well known that these intermetallic particles will form micro galvanic cells with the aluminum matrix.[15–17] In other words, the large number of intermetallic particles result in a galvanic coupling with the aluminum matrix with a large contact surface, resulting in high pitting corrosion activity near the CLS. This inevitably means that the CLS has a large local influence on the corrosion properties of the TRC AA3003, especially on the exposed cross sections of the fin material in the heat exchangers. Therefore, this study will focus on cross-sectional samples.

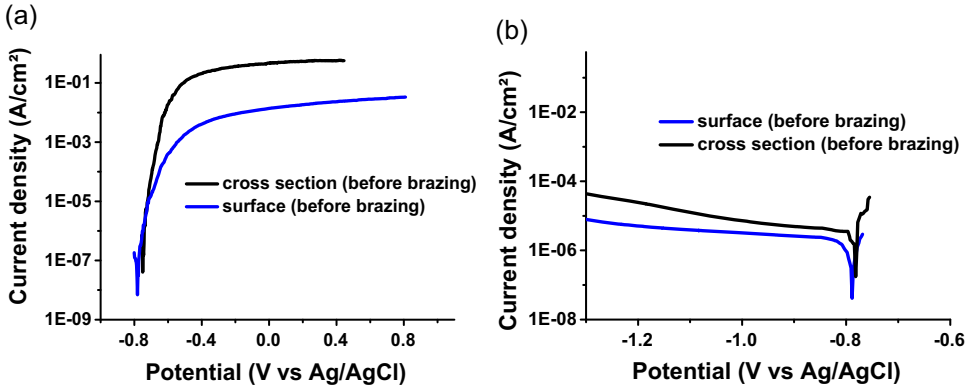

FIGURE 3 Anodic (a) and cathodic (b) polarization measurements in 0.1 M NaCl on the surface and cross-section of the flat-rolled TRC AA3003 material. TRC, twin roll casting [Color figure can be viewed at wileyonlinelibrary.com]

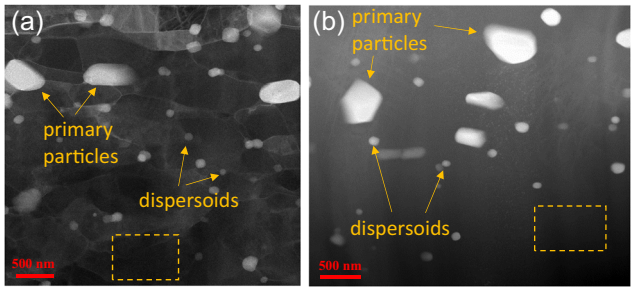

FIGURE 4 HAADF-STEM images of the cross-sectional samples (a) before and (b) after the simulated brazing step. The dashed yellow rectangles mark the areas used in determining the chemical composition of the matrix. HAADF-STEM, high angle annular dark field-scanning TEM [Color figure can be viewed at wileyonlinelibrary.com]

3.2 | Effect of simulated brazing on the microstructure

HAADF-STEM/EDS measurements were conducted to gain insights into the influence of simulated brazing on the microstructures of these specimens. This is shown in Figure 4, with cross-sectional samples. Figure 4a shows that the microstructure before the simulated brazing step has a large grain boundary density. Before simulated brazing there are two types of intermetallic particles: primary particles and dispersoids. The primary particles consist out of two types of eutectically formed intermetallics: the α-Al(Mn,Fe)Si phase, typically $Al_{15}(Mn,Fe)_3Si_2$, and the Al(Mn,Fe) phase, typically $Al_6(Mn,Fe)$.[10] The primary particles vary in size but are generally >0.5 μm in diameter and are rich in Fe, as can be seen in the SEM/EDS-spectrum of Figure 5. The dispersoids are smaller and, in general, in between 0.1 and 0.5 μm in diameter. These particles are rich in Mn, contain Si and contain only small amounts of Fe, as can be seen in the corresponding SEM/EDS-spectrum in Figure 5. These particles are most likely formed by a solid-state reaction and are known as α-AlMnSi-type dispersoids, typically as α-$Al_{12}Mn_3Si_{1\text{-}2}$.[10] The microstructure after simulated brazing is shown in Figure 4b. This image shows a coarse grain structure, with a low grain boundary density. This suggests that possible recrystallization took place as a result of the simulated brazing step. The composition of the intermetallic particles remained the same after the simulated brazing step. The high-resolution EDS-analysis reveals a slight increase of Si content in the matrix after simulated brazing, as can be seen in Table 2. The dashed yellow rectangles in Figure 4 mark the areas used in the determination of the chemical composition of the matrix. Although X-rays were being collected for a moderately long period (1 hr), poor counting statistics were acquired for Mg, Cu L-series and Zr as they exist at minor levels within the matrix. Thus, to avoid any unreliable quantifications, Mg, Cu, and Zr are not considered. It is well known that the α-AlMnSi-type dispersoids start to dissolve at high temperatures, like for instance a

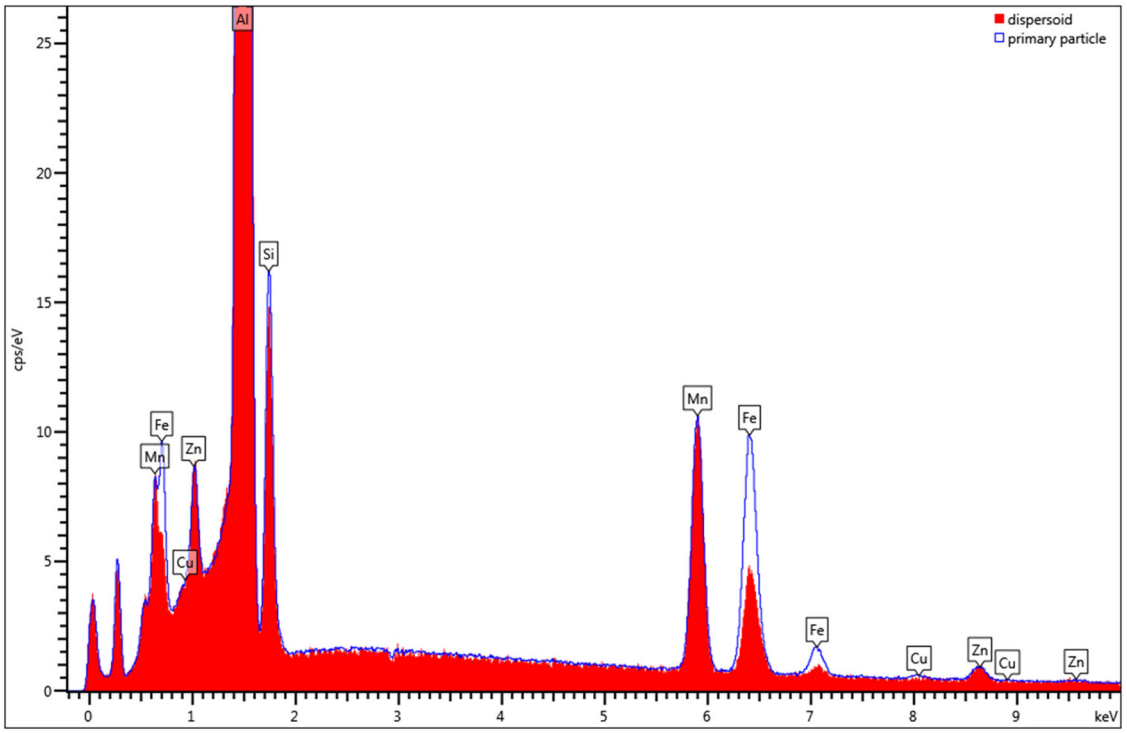

FIGURE 5 SEM/EDS spectra of typical primary intermetallic particles and the dispersoids after brazing. SEM/EDS, scanning electron microscopy/energy dispersive X-ray spectroscopy [Color figure can be viewed at wileyonlinelibrary.com]

TABLE 2 The chemical composition of the matrix before and after brazing, obtained by HAADF-STEM/EDS

Type	Zn (wt%)	Si (wt%)	Fe (wt%)	Mn (wt%)	Al (wt%)
Before brazing	1.18	0.15	0.05	0.05	Balance
After brazing	0.93	0.37	0.05	0.04	Balance

Abbreviations: EDS, energy dispersive X-ray spectroscopy; HAADF-STEM, high angle annular dark field-scanning TEM.

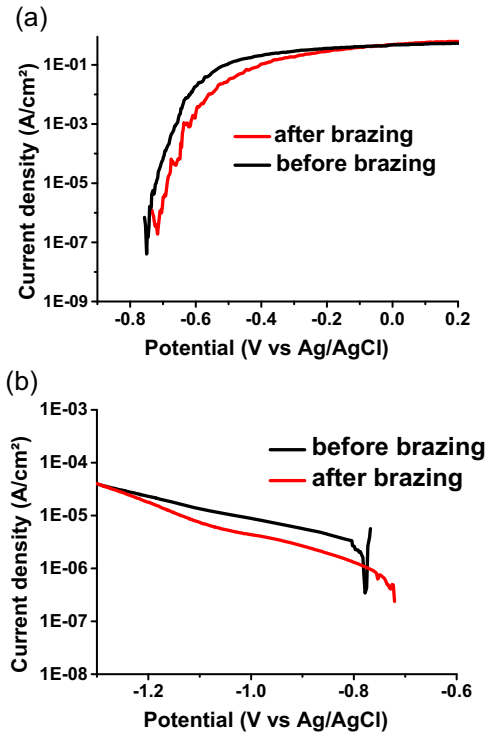

FIGURE 6 Anodic (a) and cathodic (b) potentiodynamic polarization measurements in 0.1 M NaCl, showing the effect of simulated brazing on cross-sectional TRC AA3003 samples. TRC, twin roll casted [Color figure can be viewed at wileyonlinelibrary.com]

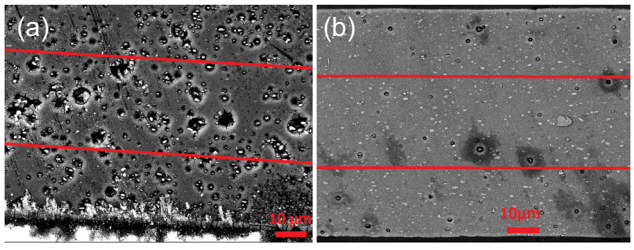

FIGURE 7 SEM images of cross-sectional TRC AA3003 samples before (a) and after (b) simulated brazing immersed in 0.1 M NaCl, the centre line segregation (CLS) is marked with two parallel red lines. SEM, scanning electron microscopy; TRC, twin roll casted [Color figure can be viewed at wileyonlinelibrary.com]

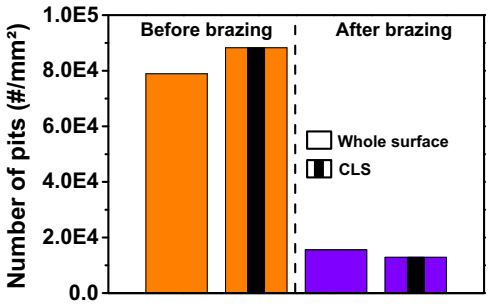

FIGURE 8 Number of pits per surface area for the whole cross section and for the CLS region of the TRC AA3003 cross-section before and after simulated brazing [Color figure can be viewed at wileyonlinelibrary.com]

brazing step at 600°C.[18] The slight increase of Si content in the matrix, seen in Table 2, is most likely caused by this partial dissolution of the α-AlMnSi-type dispersoids, during simulated brazing.

3.3 | Effect of simulated brazing on the pitting behavior

Potentiodynamic polarization measurements were performed on cross-sectional samples before and after a simulated brazing step in aerated solution. The anodic polarization measurements showed an active behavior for both samples and the anodic limiting current density does not change significantly after the simulated brazing step, as shown in Figure 6a. In aerated solution, the pitting potential coincides with the corrosion potential. At this potential value, the lowest current density is measured. By increasing the applied potential a rapid increase in current density (as a result of the pitting process) can be clearly noticed. The pitting potential is shown to slightly increase after the simulated brazing step. On average, the pitting potential of the cross-sectional samples before simulated brazing is -0.77 ± 0.02 V (vs. Ag/AgCl) and after simulated brazing -0.71 ± 0.01 V (vs. Ag/AgCl). The cathodic polarization measurements showed that the cathodic current densities are slightly lower after a simulated brazing step, as can be seen in Figure 6b. The partial dissolution of the α-AlMnSi-type dispersoids causes a slight reduction in surface area of α-AlMnSi-type dispersoids. Lowering the surface area of the α-AlMnSi-type dispersoids can result in a decrease in cathodic activity and thus also a decrease in the cathodic current densities, as seen in the cathodic polarization plots of Figure 6b. Furthermore, these measurements also showed a slight increase of the pitting potential after a simulated brazing step. This indicates a slight increase in pitting resistance after the brazing step. The slight increase in pitting potential after simulated brazing suggests that the simulated brazing step is causing a change in the galvanic cell that is formed between

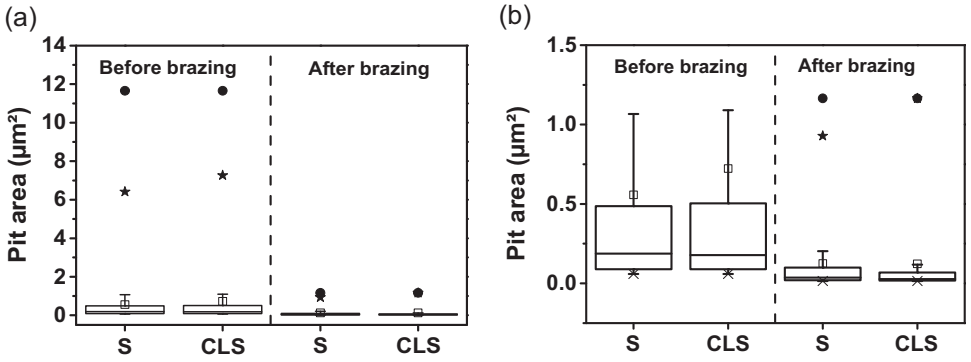

FIGURE 9 (a) Boxplots of the area size of the formed pits for the whole TRC AA3003 cross section and for the CLS region of the cross-section before and after simulated brazing, (b) zoom of the boxplots. (•) represents the maximum, (★) represents the 99th percentile and (□) represents the average. CLS, centre line segregation; TRC, twin roll casted

the intermetallic particles and the surrounding aluminum matrix. This could indicate that the driving force for pitting corrosion due to the galvanic coupling is reduced after the brazing step.

3.4 | Effect of simulated brazing on the corrosion morphology

Cross-sectional samples before and after a simulated brazing step were immersed in a 0.1 M NaCl solution for 24 hr. The corrosion morphology of these immersed samples is shown in Figure 7. These SEM images indicate a significant degree of pitting corrosion before simulated brazing with a particularly high activity at the CLS showing larger pits, marked by the red lines. However, after the simulated brazing step, the amount of pitting corrosion activity is greatly reduced throughout the whole cross-section. Figure 8 reports the number of pits per surface area for the whole cross section and for the CLS part of the cross section before and after simulated brazing. This figure shows that after brazing about four times less pits are created per surface area. Furthermore, the number of pits per surface area is slightly higher at the CLS compared to that for the whole cross section before simulated brazing. After a simulated brazing step the number of pits per surface area is about the same for both the whole cross section and at the CLS. The boxplots of Figure 9 report the area size of the formed pits for the whole cross section and for the CLS part of the cross-section before and after simulated brazing. The boxplots

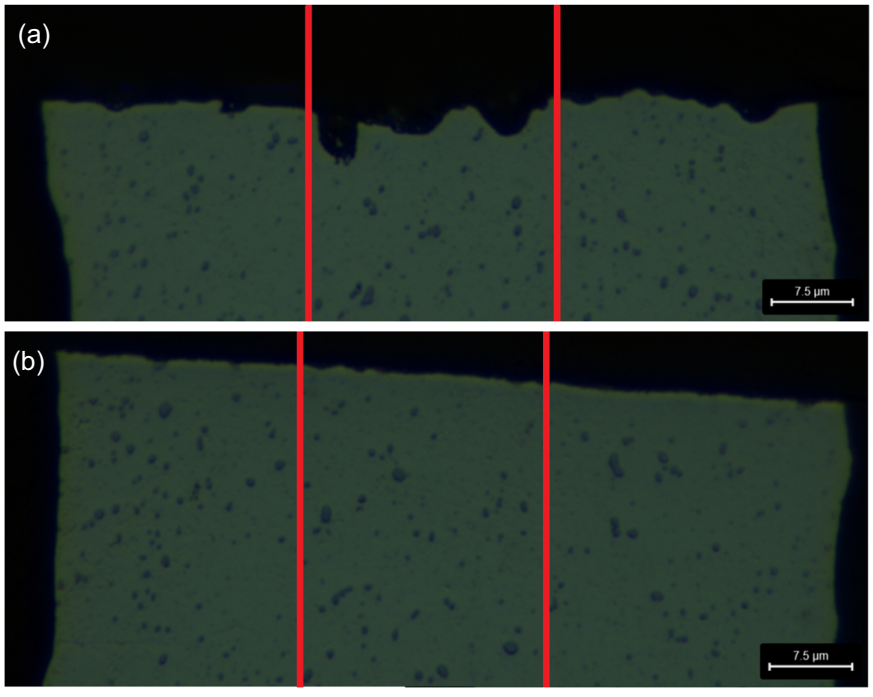

FIGURE 10 Optical micrographs of cross sections of immersed TRC AA3003 cross-sectional samples before (top) and after (bottom) simulated brazing, the CLS is marked with two parallel red lines. CLS, centre line segregation; TRC, twin roll casted [Color figure can be viewed at wileyonlinelibrary.com]

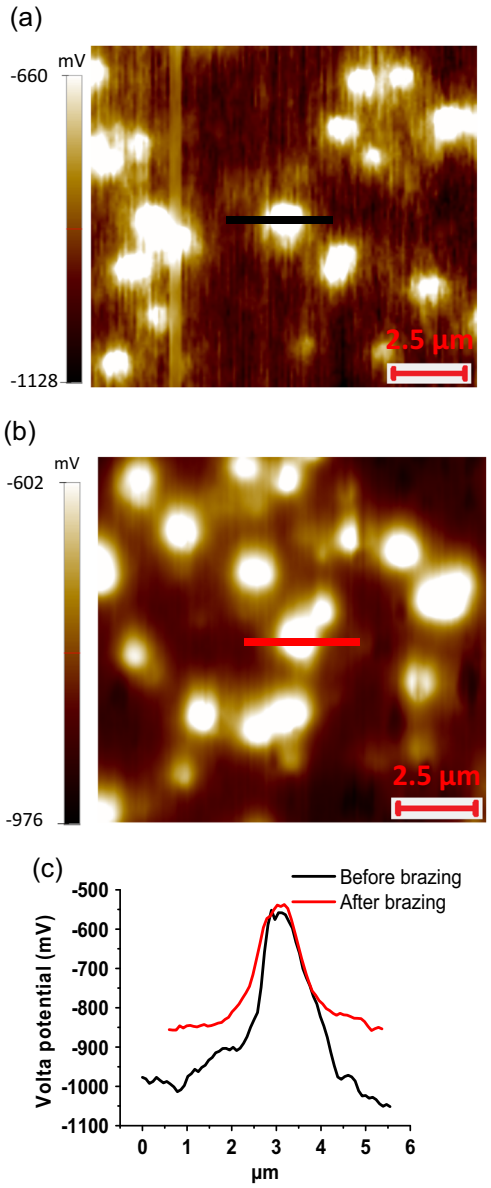

FIGURE 11 Volta potential maps of cross-sectional samples before (a) and after (b) simulated brazing. Line scans (c) of the Volta potential maps covering two intermetallic particles, of about the same size, and the surrounding aluminum matrix [Color figure can be viewed at wileyonlinelibrary.com]

of the whole cross-section and of the CLS show almost no difference, this before and after simulated brazing, meaning that most of the larger pits are all near the CLS, as was also seen in the SEM images in Figure 7. Moreover, the boxplots report that before simulated brazing the average area of the pits is larger and that there is a higher number of above average sized pits.

Cross sections of the immersed cross-sectional samples from Figure 7, are shown in Figure 10. These optical micrographs show a higher penetration depth before simulated brazing, especially at the CLS marked in the optical micrographs by the red lines. This higher pitting corrosion activity at the CLS is most likely due to a large number of intermetallic particles per surface area. In other words, the large number of intermetallic particles results in a galvanic coupling with the aluminum matrix with a large contact surface, resulting in the relatively high pitting corrosion activity near the CLS.

3.5 | Effect of simulated brazing on the interaction between the intermetallic particles and the aluminum matrix

Volta potential maps of cross-sectional samples before and after simulated brazing were made by use of SKPFM. The maps of the cross-sectional samples covered both the CLS and the adjacent zones in the cross-section. In this way zones with and without CLS are measured, so that the maps are representative for the whole cross-section. Examples of these Volta potential maps are given in Figure 11. They show that the intermetallic particles have a higher nobility compared to the aluminum matrix. This cathodic behavior of the intermetallic particles was also shown by Davoodi et al.[8–10]

Figure 12 shows examples of histograms of the Volta potentials measured in the Volta potential maps of the cross-sectional samples before and after a simulated brazing step. The statistical distribution of these Volta potentials is shown in Figure 12 to be asymmetric. This asymmetry is due to the fact that the overall Volta potential consists of two main contributions. The first contribution is from the Volta potential of the aluminum matrix, which is the most abundant phase and is determining the position of the main peak. The second contribution is from the Volta potential of the intermetallic particles. This second contribution causes the broad tail of the potential distribution. This is because the intermetallic particles do not all have the same size, but rather have a size distribution. Since it is known that these intermetallic particles with different sizes will have different Volta potentials,[10] the distribution in size will cause distribution in Volta potentials and thus cause the broad tail in the histograms shown in Figure 12. Furthermore, Figure 12 shows that the Volta potential of the aluminum matrix increases about 124 ± 22 mV after the simulated brazing step. In other words, the simulated brazing step causes the Volta potential of the matrix to shift in the cathodic direction. The shift of the Volta potential of the aluminum matrix could be caused by the slight increase of Si content in the matrix after simulated brazing. The slight enrichment in Si could originate from the partial dissolution of α-AlMnSi-type dispersoids during brazing.

A statistical analysis of the Volta potential difference between the intermetallic particles and the aluminum matrix was carried out. The average Volta potential value of the intermetallics was determined from the histogram

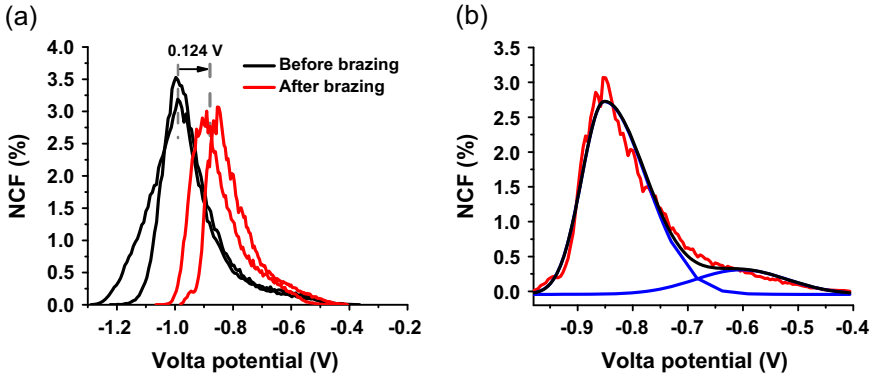

FIGURE 12 (a) Potential distribution of the Volta potential maps of cross-sectional TRC AA3003 samples before and after simulated brazing, with NCF (normalized count frequency) in percent and CPD (contact potential difference) in Volt. (b) Deconvolution of the histograms shows the two main contributions. TRC, twin roll casted [Color figure can be viewed at wileyonlinelibrary.com]

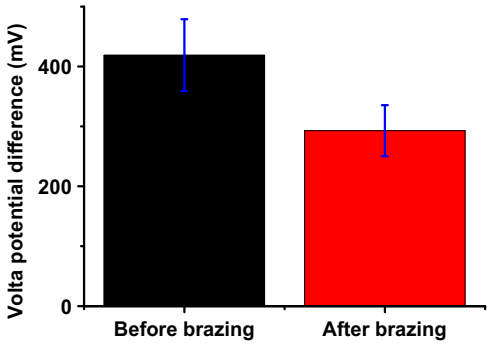

FIGURE 13 Volta potential difference between the intermetallic particles and the aluminum matrix before and after simulated brazing, in cross-sectional TRC AA3003 samples. TRC, twin roll casted [Color figure can be viewed at wileyonlinelibrary.com]

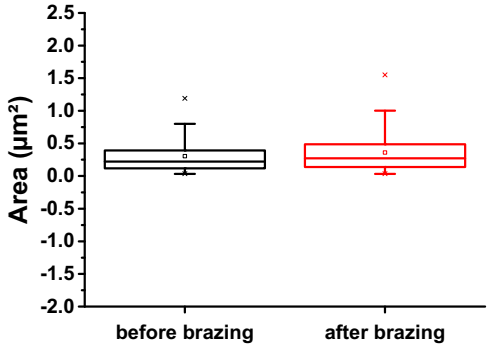

FIGURE 14 Box plots of the area size of the intermetallic particles before and after simulated brazing of the twin roll cast AA3003 [Color figure can be viewed at wileyonlinelibrary.com]

of all Volta potentials measured on intermetallic particles, while the average Volta potential of the matrix was obtained from the histograms of the Volta potential maps acquired in large areas. Figure 13 shows this difference between the Volta potentials of the intermetallic particles and the aluminum matrix in the cross-sectional samples before and after a simulated brazing step. This Volta potential difference decreases about 120 mV after the simulated brazing step. This is in agreement with the shift of the Volta potential of the aluminum matrix towards the cathodic direction after simulated brazing. This decrease in Volta potential difference between the intermetallic particles and the surrounding aluminum matrix after simulated brazing is also shown in the line scans performed on the Volta potential maps of Figure 11. These line scans cover two intermetallic particles of about the same size before and after the simulated brazing step and are shown in Figure 11. It is well known that the size of the intermetallic particles influences the value of their Volta potential. Davoodi et al.[10] attributed the size dependence of the Volta potential of the intermetallic particles to a variation in Fe and Si content in these particles. Nevertheless, the box plots in Figure 14 show that the average size of the intermetallic particles remains approximately the same after the simulated brazing step. Besides the decrease of the Volta potential difference between the aluminum matrix and the intermetallic particles, in addition, a correlation between the corrosion potential and the Volta potential is reported in prior literature.[19,20] However, it should be noted that some deviation of this direct correlation is possible. The corrosion potential measured in aqueous solutions might not always correlate with the Volta potentials measured in air, meaning that some care is necessary when analyzing the Volta potential maps.[21] For the present study, the Volta potential maps indicate that the electrochemical potential difference in the galvanic cells, formed between these intermetallic particles and the surrounding aluminum matrix, will also decrease and correlate to a reduction of the extent of pitting corrosion after simulated brazing. This is in agreement with the SEM-images and the optical micrographs, which clearly show less pitting after simulated brazing, especially at the

CLS. This is also in line with the observed increase in pitting potential after simulated brazing.

4 | CONCLUSION

This work studied the effect of a simulated brazing step on the microstructure and the corrosion behavior of a twin roll cast AA3003, used as fin material in heat exchangers. The following conclusions can be drawn:

- It is shown that the cross sections are significantly more active than the surface of the fin material. CLS plays a major role in the corrosion behavior of these specimens.
- The pitting corrosion activity and penetration depth of the formed pits decreased considerably after the simulated brazing step, especially near the CLS.
- The simulated brazing step reduces the grain boundary density in the cross sections and causes a slight increase of Si content in the matrix.
- The SKPFM measurements showed that after simulated brazing the CPD between the intermetallic particles and the aluminum matrix reduced significantly. This is due to the increase in the nobility of the matrix, possibly caused by a slight increase of the Si content in the matrix after simulated brazing.

To conclude, it is shown that the simulated brazing step applied improved the pitting corrosion resistance of TRC 3003 AA fin material.

ORCID

Donovan Verkens http://orcid.org/0000-0003-2208-0892

REFERENCES

[1] Z. Lv, F. Du, Z. An, H. Huang, Z. Xu, J. Sun, *J. Alloys Compd.* **2015**, *643*, 270.
[2] Y. Birol, *J. Alloys Compd.* **2009**, *486*, 168.
[3] D. Altenpohl, *Aluminium Viewed from Within*, Aluminium-Verlag GmbH, Düsseldorf **1982**.
[4] M. Poková, M. Cieslar, M. Slámová, *Int. J. Mater. Res.* **2009**, *100*, 391.
[5] Y. Liu, M. F. Frolish, W. M. Rainforth, X. Zhou, G. E. Thompson, G. M. Scamans, J. A. Hunter, *Surf. Interface Anal.* **2010**, *42*, 180.
[6] F. N. Afshar, A. M. Glenn, J. H. W. De Wit, H. Terryn, J. M. C. Mol, *Electrochim. Acta* **2013**, *104*, 48.
[7] S. Y. Paredes-Dugarte, B. Hidalgo-Prada, *Procedia Mater. Sci.* **2015**, *8*, 82.
[8] A. Davoodi, J. Pan, C. Leygraf, S. Norgren, *Electrochim. Acta* **2007**, *52*, 7697.
[9] A. Davoodi, J. Pan, C. Leygraf, S. Norgren, *J. Electrochem. Soc.* **2008**, *155*, C138.
[10] A. Davoodi, J. Pan, C. Leygraf, S. Norgren, *J. Electrochem. Soc.* **2008**, *155*, C211.
[11] F. N. Afshar, J. H. W. De Wit, H. Terryn, J. M. C. Mol, *Electrochim. Acta* **2013**, *88*, 330.
[12] C. Işıksaçan, M. Günyüz, O. Birbaşar, C. Konya, M. Dündar, *Mater. Sci. Forum* **2014**, *794–796*, 181.
[13] J. H. W. De Wit, *Electrochim. Acta* **2004**, *49*, 2841.
[14] P. Schmutz, *J. Electrochem. Soc.* **1998**, *145*, 2285.
[15] R. G. Buchheit, *J. Electrochem. Soc.* **1995**, *142*, 3994.
[16] N. Birbilis, R. G. Buchheit, *J. Electrochem. Soc.* **2005**, *152*, B140.
[17] S. Paredes-Dugarte, B. Hidalgo-Prada, R. Avila-Godoy, M. Briceno-Valero, *Rev. Tec. La Fac. Ing. Univ. Del Zulia* **2007**, *30*, 168.
[18] Y. J. Li, L. Arnberg, *Acta Mater.* **2003**, *51*, 3415.
[19] V. Guillaumin, P. Schmutz, G. S. Frankel, *J. Electrochem. Soc.* **2001**, *148*, B163.
[20] M. Rohwerder, E. Hornung, M. Stratmann, *Electrochim. Acta* **2003**, *48*, 1235.
[21] C. Örnek, D. L. Engelberg, *Corros. Sci.* **2015**, *99*, 164.

How to cite this article: Verkens D, Revilla RI, Kosari A, et al. Effect of simulated brazing on the microstructure and corrosion behavior of twin roll cast AA3003. *Materials and Corrosion*. 2020;71:60–69. https://doi.org/10.1002/maco.201911053